The International Journal of Advanced Manufacturing Technology (2023) 126:3133–3148
https://doi.org/10.1007/s00170-023-11275-7

ORIGINAL ARTICLE

# High-efficiency abrasive water jet milling of aspheric RB-SiC surface based on BP neural network depth control models

Hongxing Deng[1,2] · Peng Yao[1,2,3] · Kuo Hai[4] · Shimeng Yu[1,2] · Chuanzhen Huang[5] · Hongtao Zhu[1,2] · Dun Liu[1,2]

Received: 26 December 2022 / Accepted: 13 March 2023 / Published online: 29 March 2023


## Abstract

For large processing allowance of large diameter RB-SiC mirror blanks and low efficiency of grinding, an abrasive water jet milling is used to quickly remove the processing allowance. In this article, a single kerf profile processed by abrasive water jet milling was effectively fitted to the Gaussian curve. By superimposing Gaussian curves linearly, the surface waviness of superimposed curve was gradually reduced as step-over distance decreased. The surface waviness induced by abrasive water jet milling can be effectively reduced when step-over distance is controlled to less than 1.8σ. BP neural network models between step-over distance, traverse speed, and milling depth were established. The prediction error of milling depth can be controlled at about 5% of the total depth, with a maximum error less than 7%. The aspherical RB-SiC surface was generated by abrasive water jet milling with a processing path composed of 20 spiral segments. Different milling depths were obtained by setting different levels of traverse speed and step-over distance for each spiral segment. The processed aspherical surface was highly fitted to the design aspherical surface with a maximum error about 10% of the total depth. The error curves float at the zero line, and the error curves were controlled at 20% of the total depth. By this method, the processing allowance of large diameter RB-SiC mirror blanks can be effectively reduced.

**Keywords** Abrasive water jet · RB-SiC · Aspheric processing · Depth of cut · BP neural network model

## 1 Introduction

With the development of space technology, the requirements for space optical system resolution continue to increase [1, 2]. According to the diffraction theory of optical system, the angular resolution $\alpha$ of optical system is related to wavelength $\lambda$ and aperture $D$ as $\alpha = 1.22\lambda/D$. In order to increase angular resolution, it is required to increase the aperture in the same spectrum observed [3–5]. With the increase of the aperture, the weight and transmission cost of mirrors increase dramatically, so the lightweight of large aperture mirrors is reduced. However, the lightweight reduces the mirror stiffness and increases the surface error introduced by gravity. In order to ensure the surface accuracy and lightweight at the same time, high requirements are placed on the materials of large aperture mirror blanks. RB-SiC has become a preferred material for large aperture and lightweight mirror blanks due to its outstanding mechanical properties, which include low density, high elastic modulus, high specific stiffness, low thermal expansion coefficient, and high thermal conductivity [6].

When large-aperture RB-SiC mirror blank is prepared, it is difficult to accurately control the surface shape of the blank due to the thermal expansion and contraction, which will result in the total surface error at hundreds of microns to several millimeters. The surface error of mirror blank is removed directly by grinding in traditional way. The

✉ Peng Yao
yaopeng@sdu.edu.cn

✉ Kuo Hai
824639163@qq.com

1 Center for Advanced Jet Engineering Technologies (CaJET), School of Mechanical Engineering, Shandong University, Jinan 250061, China

2 Key Laboratory of High Efficiency and Clean Mechanical Manufacture of the Ministry of Education, Jinan 250061, China

3 Shenzhen Research Institute of Shandong University, Shenzhen 518057, China

4 Fine Mechanics & Physics, Changchun Institute of Optics, Chinese Academy of Sciences, Changchun 130033, China

5 School of Mechanical Engineering, Yanshan University, Qinhuangdao 066004, Hebei, China

processing allowance can be characterized as aspheric distribution. However, SiC is a typical difficult-to-machine material due to its high hardness and high brittleness. Even if grinding with diamond grinding wheel, its material removal rate is about 1/35th that of fused silica and less than 1/50th that of glass–ceramics [7]. Meanwhile, the diamond grinding wheel is prone to wear. These lead to extremely low processing efficiency in grinding SiC.

With the increase in aperture and demand of mirrors, a new method is required to improve processing efficiency. An abrasive water jet machining is a typical noncontact processing technique that is widely and increasingly used in difficult-to-machine materials such as engineering ceramics [8], composite materials [9–11], and high strength steels [12]. With good processing ability and no tool wear, it is a good option to process RB-SiC with abrasive water jet to quickly reduce processing allowance of mirror blank.

The shape of kerf left by a single pass of abrasive water jet was studied by many scholars. Sultan et al. [13] investigated the effect of different erosion times caused by the jet shape on the kerf profile of Ti6Al4V. The results indicated that the erosion time caused by the jet shape had little effect and the jet energy distribution made the greatest impact on the shape of kerf. Carrascal et al. [14] presented that the kerf profile could be effectively fitted to the Gaussian curve and inferred as a Gaussian distribution of jet energy.

For brittle materials, the removal mechanism of abrasive water jet is complex, including the influence of impact, shear and micro-cutting of abrasive particles, the influence of heat generated by impact, and the influence of multiple erosion [15, 16]. Therefore, it is difficult to establish an accurate theoretical model to predict milling depth. Pahuja et al. [17] developed a semiempirical model to predict milling depth of Ti6Al4V-CFRP stacks. This model was proved to be more effective than multiple regression model. Mohankumar et al. [18] built a semiempirical model by using Buckingham's π theorem to predict milling depth of metal matrix composites. The average error of the model was about 15% with maximum error of 48% of the total depth. Ozcan et al. [19] proposed a model based on energy and momentum conservation, in which milling depth was related to the machinability number of materials. The average error of the model was about 15% with maximum error of 30% of the total depth by processing multiple materials including AL6061, SS301, Ti6Al4V, and SiC. Wang et al. [20] established a universal finite element model of erosive wear to simulate the effect of the impact angle, velocity, and particle penetration on the targets. The accuracy was relatively low by comparing simulation results with the experimental results. Anwar et al. [21, 22] established the abrasive water jet milled footprint model and overlapping abrasive water jet milled footprint model for Ti6Al4V by using finite element method. The average error of the models was about 10% with a maximum error of 15% of the total depth. Bui et al. [23] used a linear superposition of Gaussian curves to predict milling depth. Preliminary experiments indicated that the actual milling depth was larger than the milling depth predicted by linear superposition of Gaussian curves. An erosion factor Ke was introduced to consider the effect of secondary impact. Then, the average error could be controlled at 5% of the total depth, with a maximum error less than 13% of the total depth. However, in order to predict milling depth, a single kerf profile was required to be measured in advance, which reduced the practicability of this method.

From the literature, it is difficult to establish a theoretical model to predict milling depth, and the prediction accuracy by using multiple regression model, semiempirical model, or finite element model is not satisfactory for processing RB-SiC mirror blanks. In order to effectively reduce the processing allowance of large aperture RB-SiC mirror blank, a new method is required to improve prediction accuracy of milling depth.

In this research, the abrasive water jet milling is used to quickly reduce processing allowance of RB-SiC before grinding. The surface waviness induced by abrasive water jet milling is effectively reduced by controlling step-over distance. BP neural network models are used to improve prediction accuracy of milling depth. Aspherical RB-SiC surface is generated with a spiral path composed of 20 spiral segments on the basis of milling depth prediction by the BP neural network models. By using abrasive water jet milling, processing allowance of large diameter RB-SiC mirror blank can be effectively reduced.

## 2 Method of aspheric processing

### 2.1 Control of surface waviness

A processing path with overlapping step-over distance tends to create large surface waviness (Fig. 1) on processed surface. The surface waviness deteriorates the surface quality and increases the grinding depth of subsequent grinding, so

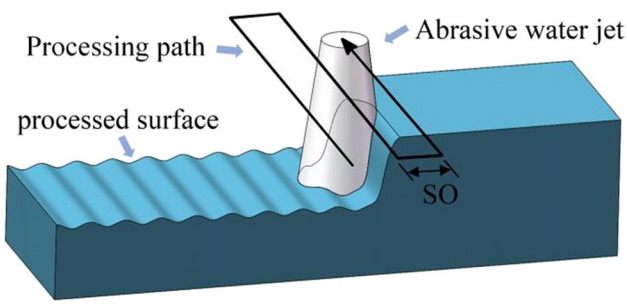


**Fig. 1** Surface waviness induced by abrasive water jet milling

it needs to be reduced during the process of abrasive water jet milling. A kerf profile (Fig. 2a) left by a single pass of abrasive water jet was modeled using a Gaussian curve. The result shows that the profile correlates well with the Gaussian curve in the middle and bottom of the kerf and a small discrepancy exists at the edge of the kerf. The adjusted $R^2$ is 0.99514, which indicates that the kerf profile can be effectively fitted to the Gaussian curve. When Gaussian fitting is performed on a single kerf profile, σ of the Gaussian curve can be obtained to represent step-over distance.

When a processing path with overlapping step-over distance is adopted, there are impact angle variation and secondary impact of abrasive, which lead to the slight variation of removal function. To simplify the model by ignoring the variations of removal function, Gaussian curves were used to replace removal function, and linear superposition (Fig. 2b) of Gaussian curves at a constant step-over distance was performed. The curves indicate that the surface waviness of superimposed curve is reduced by reducing step-over distance. When SO = 1.5σ, the surface waviness of superimposed curve is almost removed. The reduction of surface waviness is greater when the surface waviness is large, and when SO is less than 1.8σ, the reduction of surface waviness becomes gradually less significant. Combining the linear superposition of Gaussian curves with machining accuracy of abrasive water jet milling, surface waviness induced by abrasive water jet milling can be effectively reduced when the step-over distance is controlled to less than 1.8σ.

## 2.2 Selection of aspheric processing parameters

The processing allowance of mirror is nonuniform in different radial positions, and the processing allowance can be characterized as aspheric distribution. In order to remove the aspheric allowance, the milling depth needs to be variable in different positions during aspheric processing. The milling depth can be changed by changing the processing parameters, such as pressure, abrasive flow rate, standoff distance, traverse speed, and step-over distance. Different milling depths can be easily obtained by changing the pressure, but it is hard to be changed during processing. It is not a feasible way to change the milling depth by changing the pressure during processing. Because the effect of abrasive flow rate and standoff distance on milling depth is slight, it is not a suitable method to control the milling depth by control abrasive flow rate or standoff distance.

Traverse speed and step-over distance both have significant effect on milling depth. Combined that traverse speed and step-over distance are easy to change during processing by setting processing path in advance, it is feasible to obtain different milling depths by controlling traverse speed or step-over distance. In order to extend control range and improve the accuracy of milling depth, traverse speed and step-over distance are both chosen to control milling depth. From the above conclusion on the control of surface waviness, the step-over distance needs to be controlled less than 1.8σ during aspheric processing.

## 2.3 Principle of aspheric processing

The milling depth is extremely determined by the dwell time of jet. When the processing path is discontinuous or crossed, the dwell time of jet is changed, which greatly affects the milling depth; therefore, the processing path must be a continuous and uncrossed curve. The combined processing area is a ring for mirror blank, and the spiral path can be used for aspheric processing. In order to obtain different milling depths, a processing path composed of several spiral segments is used for aspheric processing. Different levels of step-over distance and traverse speed are used for each spiral segment to obtain different milling depths. As shown in Fig. 3, when the processing path is formed by adequate spiral segments, the milling depth between adjacent spiral

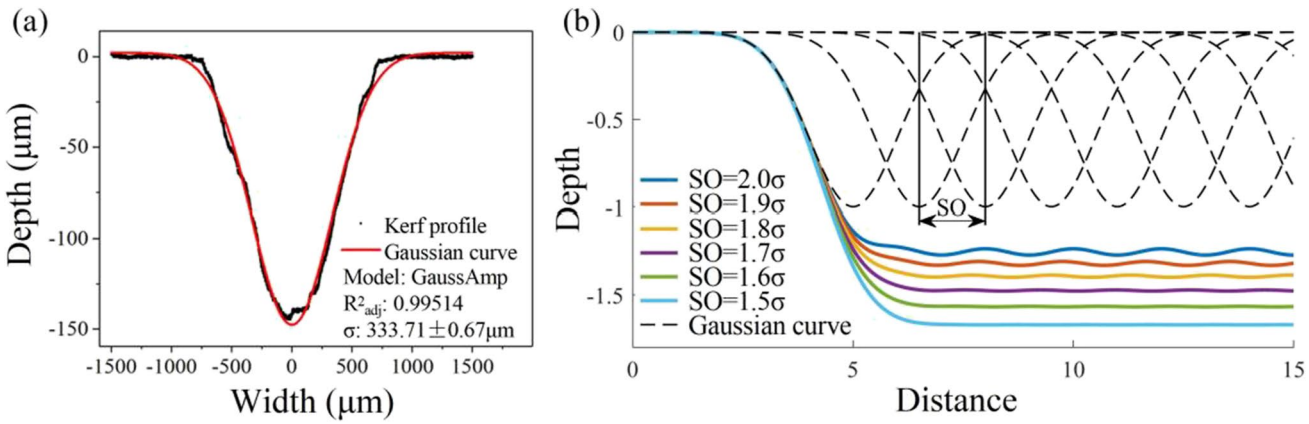


**Fig. 2** **a** Gaussian fitting and **b** linear superposition of Gaussian curves

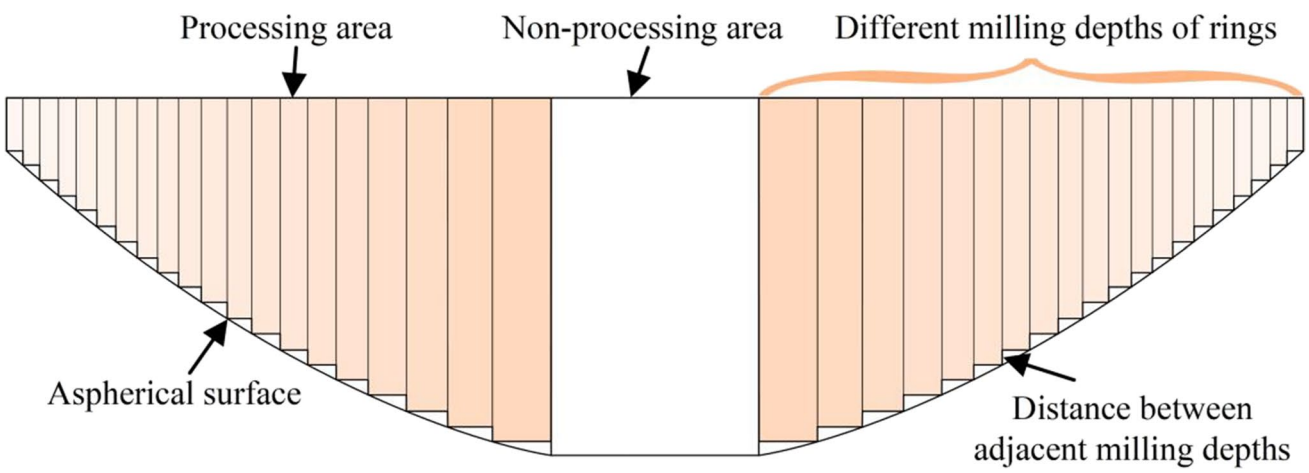


**Fig. 3** Principle of aspheric processing

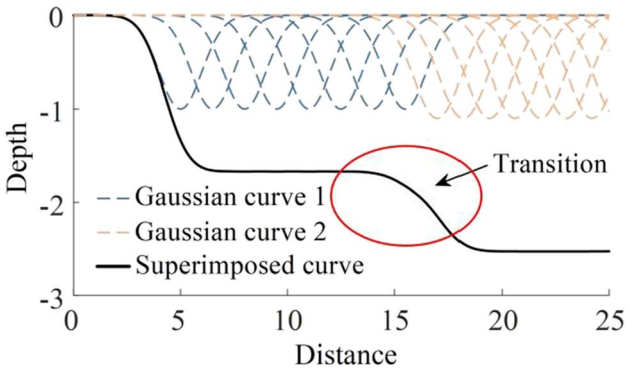


**Fig. 4** Transition of the superimposed curve with different Gaussian curves and step-over distances

segment becomes so small that the processed surface can be fitted to the design aspherical surface within error tolerance.

When traverse speed and step-over distance are changed, the shape of the Gaussian curve and step-over distance of the linear superposition are changed accordingly. The transition (Fig. 4) of superimposed curve is smooth when different Gaussian curves and step-over distances are used for linear superposition. Therefore, the transition area on the processed surface can be transformed smoothly when step-over distance and traverse speed are changed, without bumps in the transition area.

## 2.4 Milling depth control based on BP neural network models

As an error back propagation neural network, the BP neural network is composed of an input, a hidden, and an output layer. Any neuron in the front layer is connected to every neuron in the next layer, and none of the neurons in the same layer are connected. BP neural network models have good ability to fit nonlinear functions, so they can handle complex nonlinear problems and are suitable for the solutions of multi-parameter optimization [24].

The relationship of traverse speed and step-over distance to milling depth is unclear. BP neural network models can be used to establish the connection between traverse speed, step-over distance, and milling depth. Because there are only two input layer neurons, the BP neural network models with one hidden layer are used. The BP neural network model with output of step-over distance (Fig. 5a) can be obtained by setting milling depth and traverse speed as the input layer and step-over distance as the output layer. With the BP neural network model, the step-over distance required for predictive milling depth can be obtained. The BP neural network model with output of traverse speed (Fig. 5b) can be obtained by setting milling depth and step-over distance as the input layer and traverse speed as the output layer. With the BP neural network model, the traverse speed required for predictive milling depth can be obtained.

## 2.5 Protocol of aspheric processing

The flowchart for aspheric processing is shown in Fig. 6. Suitable traverse speed is assigned based on the milling depth, and the step-over distance can be obtained based on the BP neural network model with output of step-over distance. In aspheric processing, the number of spiral loops is an integer; therefore, the step-over distance needs to be adjusted according to the number of spiral loops and width of each ring. After adjusting the step-over distance, the traverse speed is adjusted according to the BP neural network model with output of traverse speed. The adjusted step-over distance and traverse speed are the final processing parameters in aspheric processing.

As shown in the dashed line in Fig. 6, after obtaining the width of each ring, the spiral loop number can be assigned

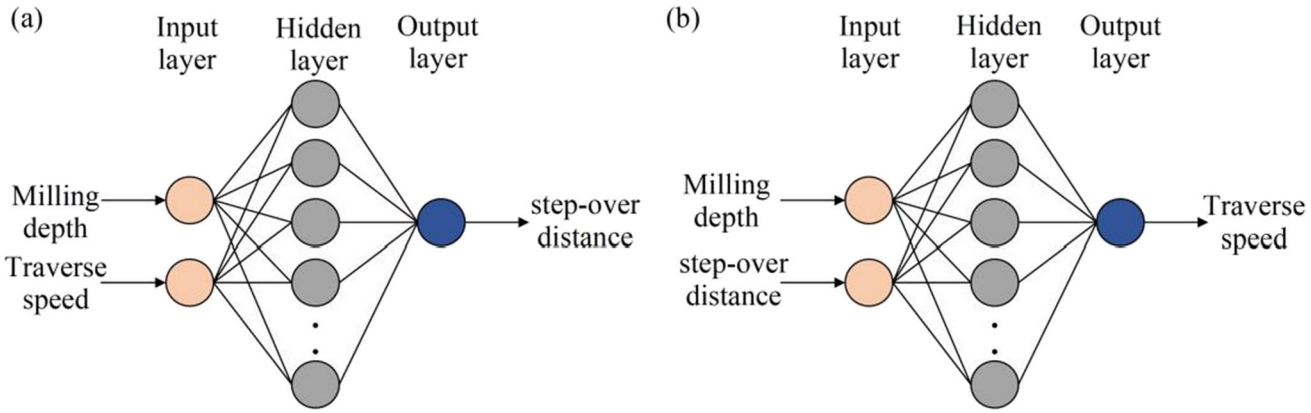


**Fig. 5** BP neural network models with output of **a** step-over distance and **b** traverse speed

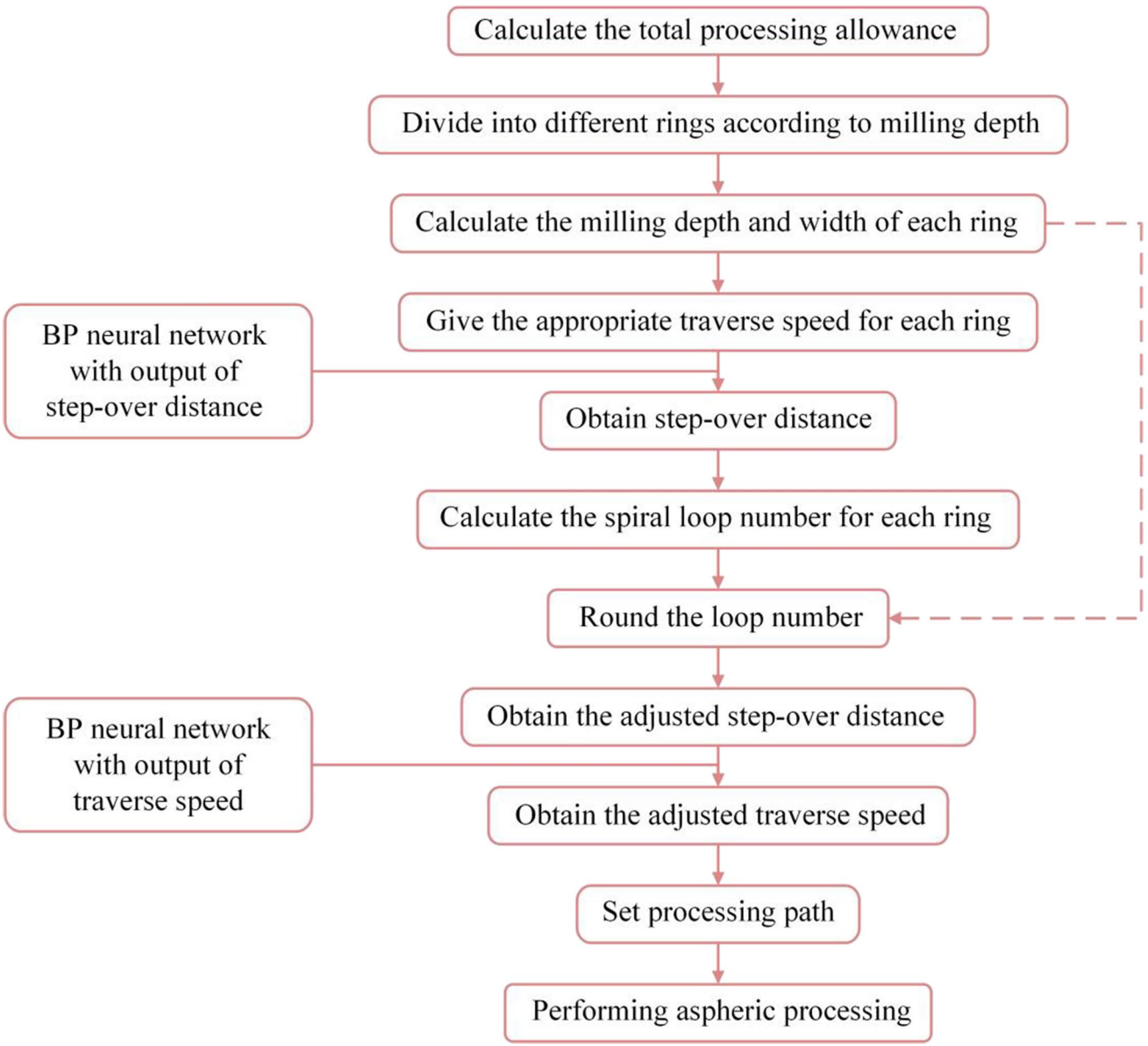


**Fig. 6** Flowchart of aspheric processing by abrasive water jet milling

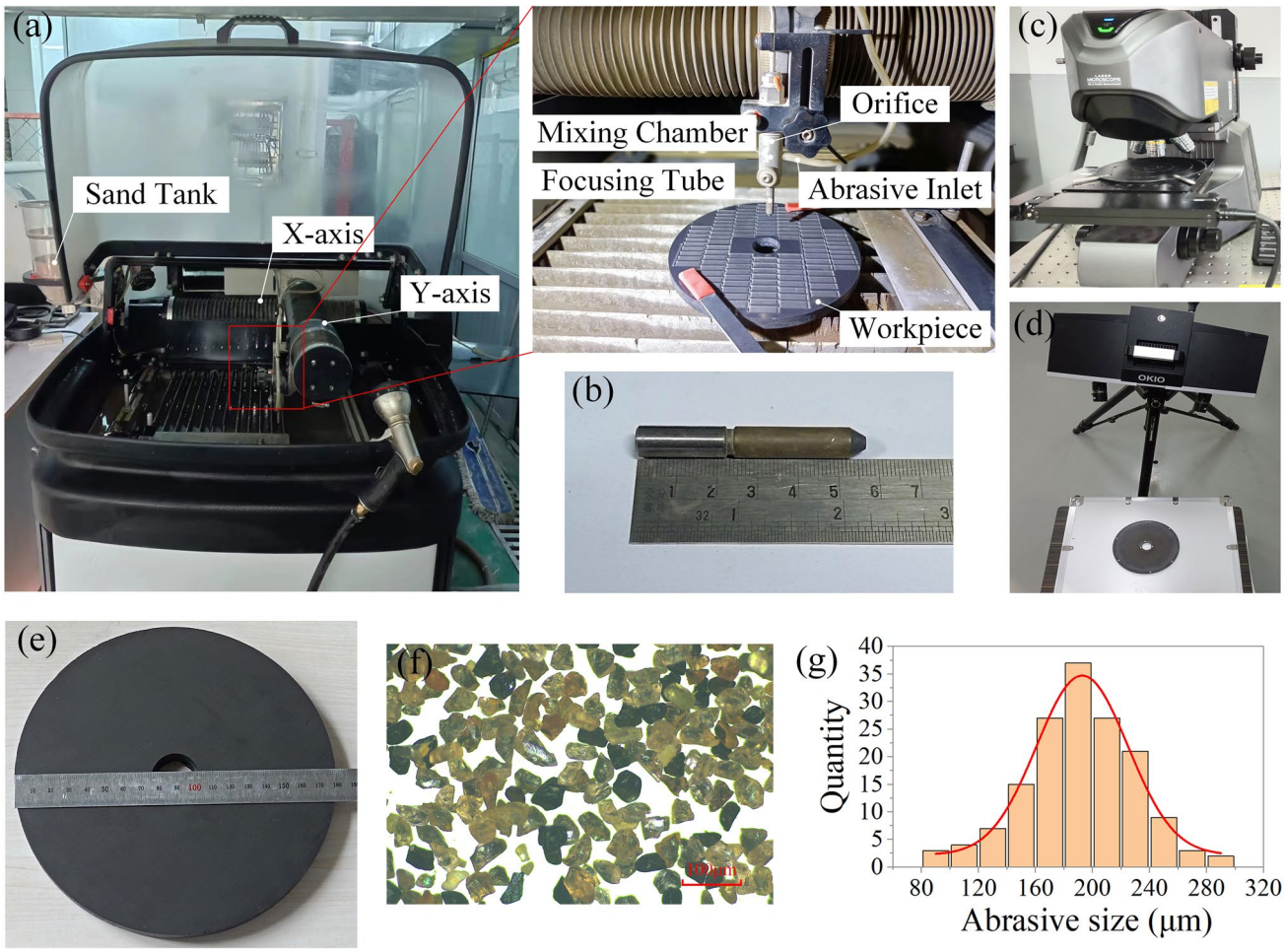


**Fig. 7** The experimental set-up and materials. **a** OMAX ProtoMAX; **b** focusing tube; **c** VK-X200K; **d** OKIO-5 M; **e** RB-SiC; **f** garnet abrasives; and **g** abrasive distribution

directly. However, traverse speed of adjacent spiral segments obtained by this method might be quite different, which results in a significant acceleration or deceleration at the joint of adjacent spiral segments.

## 3 Application of the method

### 3.1 The experimental setup and materials

Experiments were performed on an the AWJ Machine OMAX ProtoMAX (Fig. 7a) with a constant pressure of 200 MPa, an orifice diameter of 0.2 mm, a focusing tube (Fig. 7b) length of 57 mm, and a nozzle diameter of 0.76 mm. The measurement of pocket was performed using a 3D laser scanning microscope VK-X200K (Fig. 7c). The measurement of the processed aspherical surface was carried out using a noncontact blue light scanner OKIO-5 M

**Table 1** Mechanical properties of RB-SiC

| Material | Elastic modulus $E$ (GPa) | Fracture toughness $K_{IC}$ (MPa·m$^{1/2}$) | Vickers hardness Hv (GPa) |
|---|---|---|---|
| RB-SiC | 362.39 | 3.04 ± 0.56 | 20.02 ± 2.20 |

**Table 2** Processing parameters of abrasive water jet milling

| Processing parameters | Level |
|---|---|
| Traverse speed (mm/s) | 18, 21, 24, 27, 30, 33, 36, 39, 42 |
| Step-over distance (mm) | 0.20, 0.25, 0.30, 0.35, 0.40, 0.45, 0.50, 0.55, 0.60 |
| Pressure (MPa) | 200 |
| Standoff distance (mm) | 12 |
| Abrasive flow rate (g/min) | 160 |
| Size of abrasive (#) | 150 |
| Orifice diameter (mm) | 0.2 |
| Nozzle diameter (mm) | 0.76 |
| Impact angle (°) | 90 |

**Table 3** σ of Gaussian fitting at different levels of traverse speed

| Traverse speed (mm/s) | 18 | 21 | 24 | 27 | 30 | 33 | 36 | 39 | 42 |
|---|---|---|---|---|---|---|---|---|---|
| σ (μm) | 359.11 ± 0.72 | 349.68 ± 0.85 | 330.74 ± 0.52 | 334.86 ± 0.65 | 333.71 ± 0.67 | 324.12 ± 1.04 | 324.35 ± 0.66 | 319.37 ± 0.63 | 318.33 ± 1.03 |

(Fig. 7d). The material used in this study is RB-SiC (Fig. 7e). The mechanical properties are shown in Table 1. Abrasive garnet (Fig. 7f) of mesh size #150 was used in the present work to obtain acceptable surface roughness. The distribution (Fig. 7g) of abrasive size follows the Gaussian distribution.

## 3.2 Experimental data for BP neural network models

In order to develop BP neural network models, the correlation between traverse speed, step-over distance, and milling depth needs to be obtained. The processing parameters are

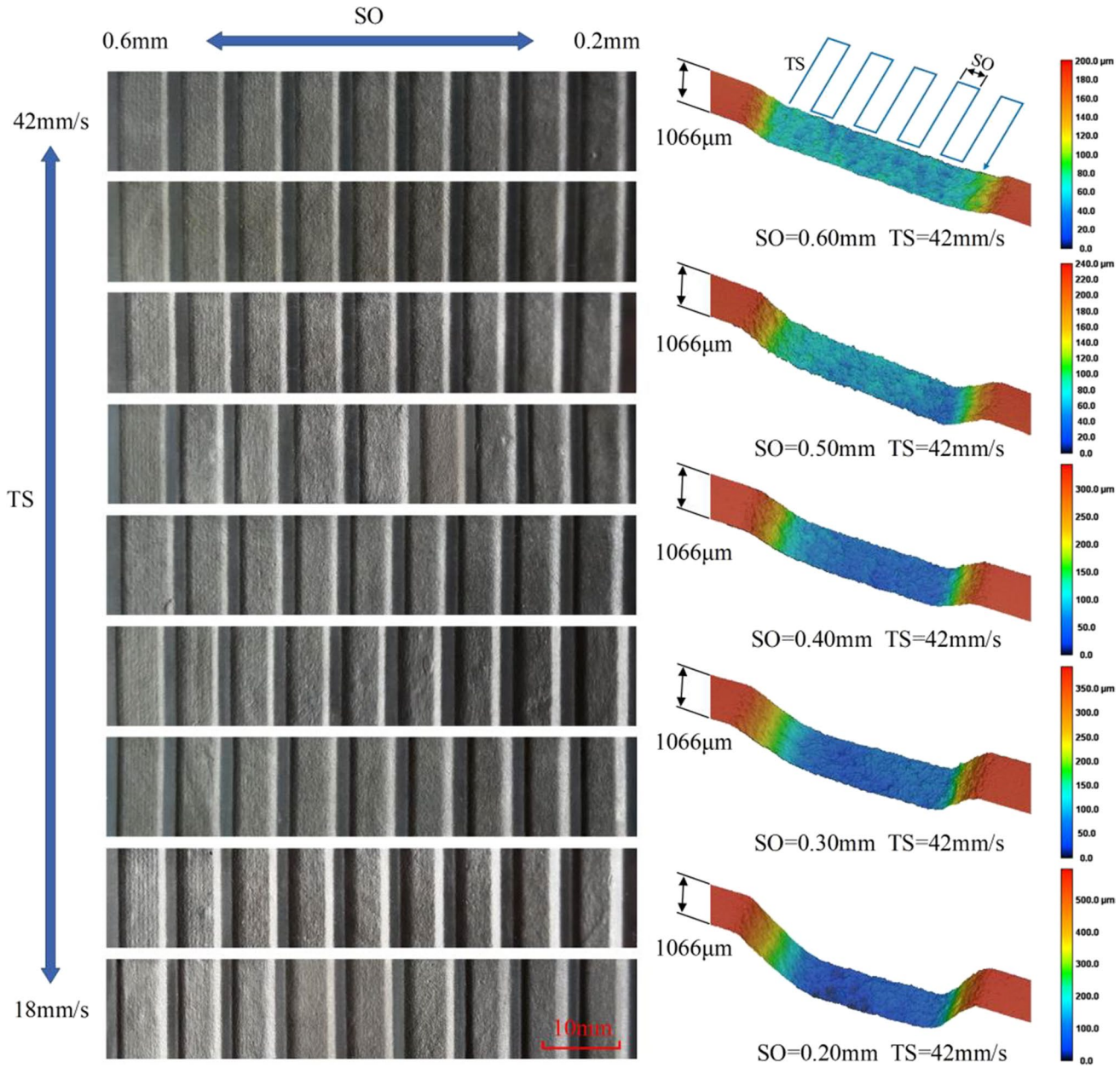


**Fig. 8** Processed pockets of RB-SiC by abrasive water jet milling

**Table 4** Experimental data for BP neural network models

| Run | TS (mm/s) | SO (mm) | Depth (μm) | Run | TS (mm/s) | SO (mm) | Depth (μm) | Run | TS (mm/s) | SO (mm) | Depth (μm) |
|---|---|---|---|---|---|---|---|---|---|---|---|
| 1 | 42 | 0.6 | 132 | 28 | 33 | 0.6 | 194 | 55 | 24 | 0.6 | 248 |
| 2 | 42 | 0.55 | 145 | 29 | 33 | 0.55 | 209 | 56 | 24 | 0.55 | 280 |
| 3 | 42 | 0.5 | 171 | 30 | 33 | 0.5 | 242 | 57 | 24 | 0.5 | 306 |
| 4 | 42 | 0.45 | 207 | 31 | 33 | 0.45 | 261 | 58 | 24 | 0.45 | 337 |
| 5 | 42 | 0.4 | 262 | 32 | 33 | 0.4 | 292 | 59 | 24 | 0.4 | 420 |
| 6 | 42 | 0.35 | 305 | 33 | 33 | 0.35 | 339 | 60 | 24 | 0.35 | 546 |
| 7 | 42 | 0.3 | 329 | 34 | 33 | 0.3 | 410 | 61 | 24 | 0.3 | 615 |
| 8 | 42 | 0.25 | 392 | 35 | 33 | 0.25 | 521 | 62 | 24 | 0.25 | 712 |
| 9 | 42 | 0.2 | 502 | 36 | 33 | 0.2 | 582 | 63 | 24 | 0.2 | 890 |
| 10 | 39 | 0.6 | 140 | 37 | 30 | 0.6 | 185 | 64 | 21 | 0.6 | 342 |
| 11 | 39 | 0.55 | 155 | 38 | 30 | 0.55 | 223 | 65 | 21 | 0.55 | 417 |
| 12 | 39 | 0.5 | 175 | 39 | 30 | 0.5 | 252 | 66 | 21 | 0.5 | 460 |
| 13 | 39 | 0.45 | 227 | 40 | 30 | 0.45 | 281 | 67 | 21 | 0.45 | 522 |
| 14 | 39 | 0.4 | 270 | 41 | 30 | 0.4 | 319 | 68 | 21 | 0.4 | 553 |
| 15 | 39 | 0.35 | 290 | 42 | 30 | 0.35 | 416 | 69 | 21 | 0.35 | 625 |
| 16 | 39 | 0.3 | 353 | 43 | 30 | 0.3 | 480 | 70 | 21 | 0.3 | 683 |
| 17 | 39 | 0.25 | 428 | 44 | 30 | 0.25 | 619 | 71 | 21 | 0.25 | 799 |
| 18 | 39 | 0.2 | 502 | 45 | 30 | 0.2 | 694 | 72 | 21 | 0.2 | 968 |
| 19 | 36 | 0.6 | 162 | 46 | 27 | 0.6 | 213 | 73 | 18 | 0.6 | 377 |
| 20 | 36 | 0.55 | 180 | 47 | 27 | 0.55 | 240 | 74 | 18 | 0.55 | 401 |
| 21 | 36 | 0.5 | 199 | 48 | 27 | 0.5 | 288 | 75 | 18 | 0.5 | 460 |
| 22 | 36 | 0.45 | 235 | 49 | 27 | 0.45 | 309 | 76 | 18 | 0.45 | 574 |
| 23 | 36 | 0.4 | 283 | 50 | 27 | 0.4 | 391 | 77 | 18 | 0.4 | 611 |
| 24 | 36 | 0.35 | 307 | 51 | 27 | 0.35 | 456 | 78 | 18 | 0.35 | 716 |
| 25 | 36 | 0.3 | 381 | 52 | 27 | 0.3 | 543 | 79 | 18 | 0.3 | 828 |
| 26 | 36 | 0.25 | 478 | 53 | 27 | 0.25 | 694 | 80 | 18 | 0.25 | 904 |
| 27 | 36 | 0.2 | 540 | 54 | 27 | 0.2 | 851 | 81 | 18 | 0.2 | 1091 |

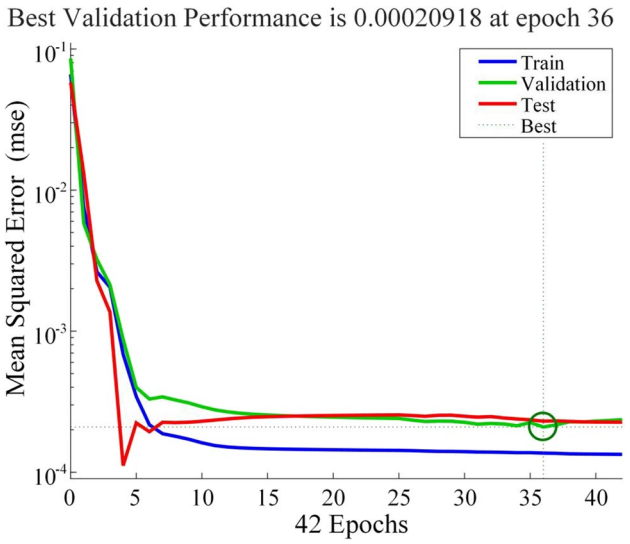


**Fig. 9** Training curves for the BP neural network model with output of step-over distance

specified in Table 2. The kerf processed by a single pass was performed at nine different levels of traverse speed, and the Gaussian fitting of its profile was proposed to obtain σ. As shown in Table 3, the variation in traverse speed has a small influence on σ. This is a result of the small influence of traverse speed on milling width. Through the above analysis of controlling surface waviness, the maximum step-over distance was controlled to less than 1.8σ that is about 0.6 mm.

Traverse speed and step-over distance were set at nine different levels to accomplish a total 81 samples of experiments. Each sample was processed following a raster scan path to create a pocket of 24 mm of length and 6 mm of width. The bottom of each pocket was flat to ensure accurate measurement on milling depth. The processed pockets of 81 samples were shown in Fig. 8. It can be found that the above method of surface waviness control is effective because there is no obvious surface waviness on the bottom of the pocket.

Three areas of each pocket were measured, respectively, the middle area, the front, and back areas at a distance of 3 mm from the middle, to obtain milling depth. A total of 21 profiles at each interval of 10 μm were measured for

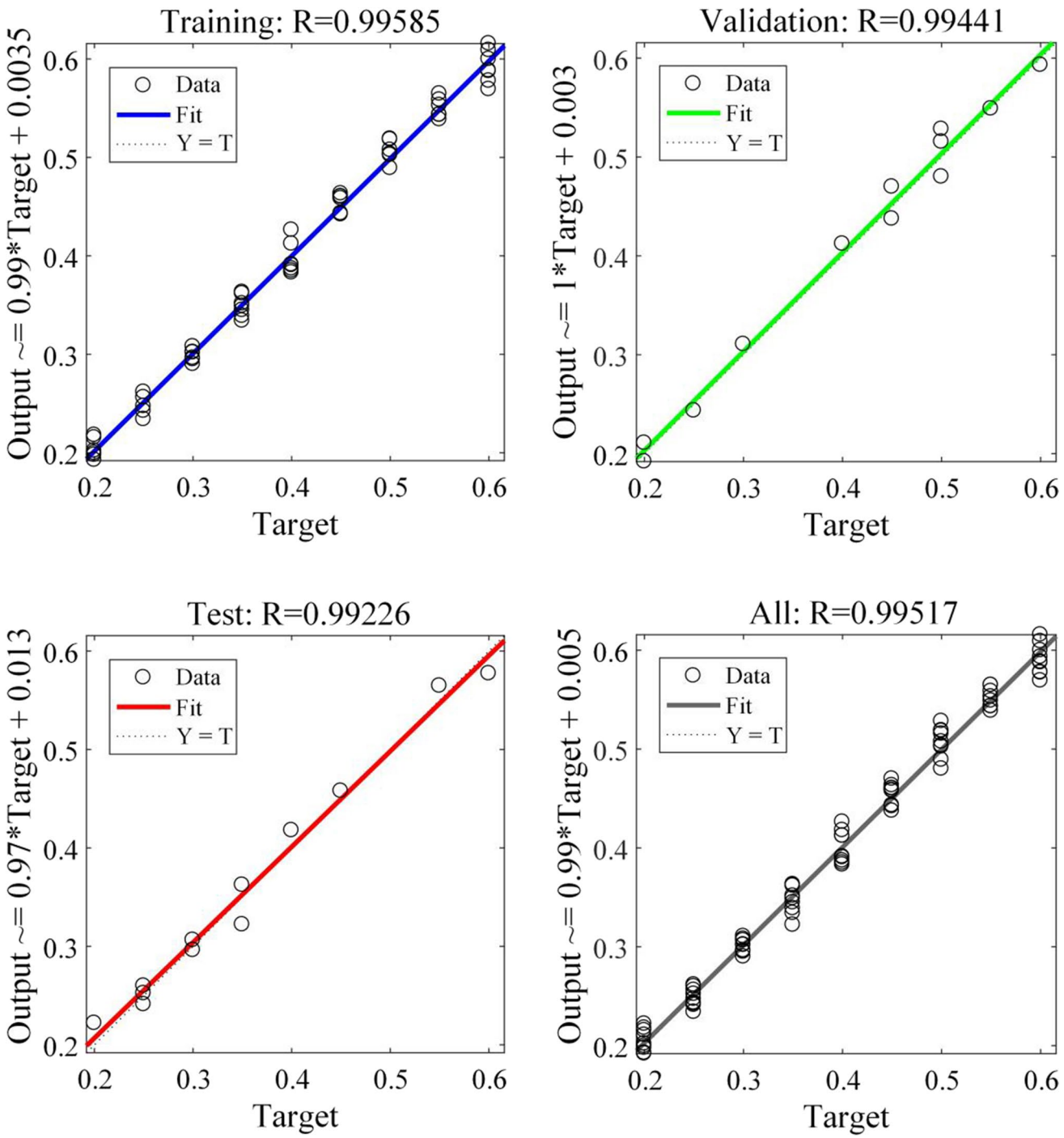


**Fig. 10** Regression analysis of the BP neural network model with output of step-over distance

each area to form an average profile. The milling depth was obtained by averaging the milling depths of each pocket. The milling depths are recorded in Table 4. With the decrease of traverse speed, the milling depth increases, and the increase rate gradually grows. Therefore, variation of traverse speed at high traverse speed results in a slight change in milling depth, and variation of traverse speed at low traverse speed leads to a sharp change in milling depth. With the decrease of step-over distance, the milling depth increases, and the increase rate gradually grows. Therefore, variation of step-over distance at high step-over distance results in a slight change in milling depth, and variation of step-over distance at low step-over distance leads to a sharp change in milling depth. These are related to the dwell time of the jet on the material.

**Table 5** Validation experiments of the BP neural network model with output of step-over distance

| Run | Predictive milling depth (μm) | Traverse speed (mm/s) | Predictive step-over distance (mm) | Measured milling depth (μm) | Error |
|---|---|---|---|---|---|
| 1 | 350 | 40 | 0.299 | 363 | 3.71% |
| 2 | 420 | 28 | 0.361 | 435 | 3.57% |
| 3 | 550 | 19 | 0.450 | 521 | 5.27% |
| 4 | 180 | 38 | 0.527 | 188 | 4.44% |
| 5 | 650 | 24 | 0.276 | 615 | 5.38% |
| 6 | 410 | 31 | 0.336 | 401 | 2.20% |
| 7 | 320 | 23 | 0.535 | 328 | 2.50% |
| 8 | 270 | 35 | 0.413 | 256 | 5.19% |

Due to linear variation of traverse speed and step-over distance, the proportion of samples of small milling depth is greater than those of large milling depth, and the prediction accuracy should be higher when the milling depth is small. Most of the milling depths are in the range of 150 to 800 μm, and the prediction accuracy within this range is relatively reliable. For milling depths outside of this range, prediction accuracy is not reliable due to insufficient experimental samples.

### 3.3 Validation of the BP neural network model with output of step-over distance

The BP neural network model with output of step-over distance was established based on the above experimental data by setting milling depth and traverse speed as the input layer and step-over distance as the output layer. The 81 samples were randomly divided into three sections for training, validation, and testing. A total of 57 samples were used for training and presented to the network, which is adjusted according to its error. In addition, 12 samples were used for validation and used to measure network generalization, and 12 samples were used for testing and provided an independent measure of network performance. The mean square error (Fig. 9) of the validation curve is minimized on 36 iterations. The regression analysis for training, validation, test, and overall is presented in Fig. 10. The BP neural network model is quite reliable because the correlation coefficient $R$ is quite close to 1.

In order to validate the prediction accuracy of the model, 8 groups of validation experiments were performed. The milling depth and traverse speed used in the validation experiments were randomly assigned within the prediction range of the BP neural network model. As shown in Table 5, the error between predictive milling depth and measured milling depth can be controlled to less than 6% of the total milling depth. With the BP neural network model, the step-over distance required for predictive milling depth can be obtained accurately.

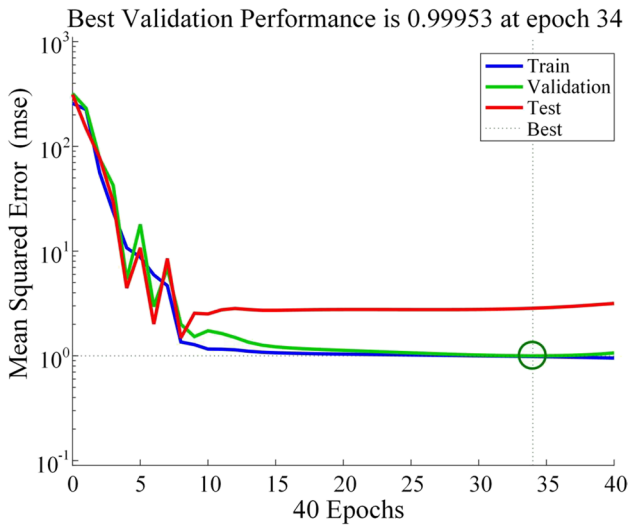


**Fig. 11** Training curves for the BP neural network model with output of traverse speed

### 3.4 Validation of the BP neural network model with output of traverse speed

The BP neural network model with output of traverse speed was established based on the above experimental data by setting milling depth and step-over distance as the input layer and traverse speed as the output layer. In the same way, the 81 samples were randomly divided into three sections for training, validation, and testing. The mean square error (Fig. 11) of validation curve is minimized on 34 iterations. The regression analysis for training, validation, test, and overall is presented in Fig. 12. The BP neural network model is quite reliable because the correlation coefficient $R$ is quite close to 1.

In order to validate the prediction accuracy of the model, 8 groups of validation experiments were performed. The milling depth and step-over distance used in the validation

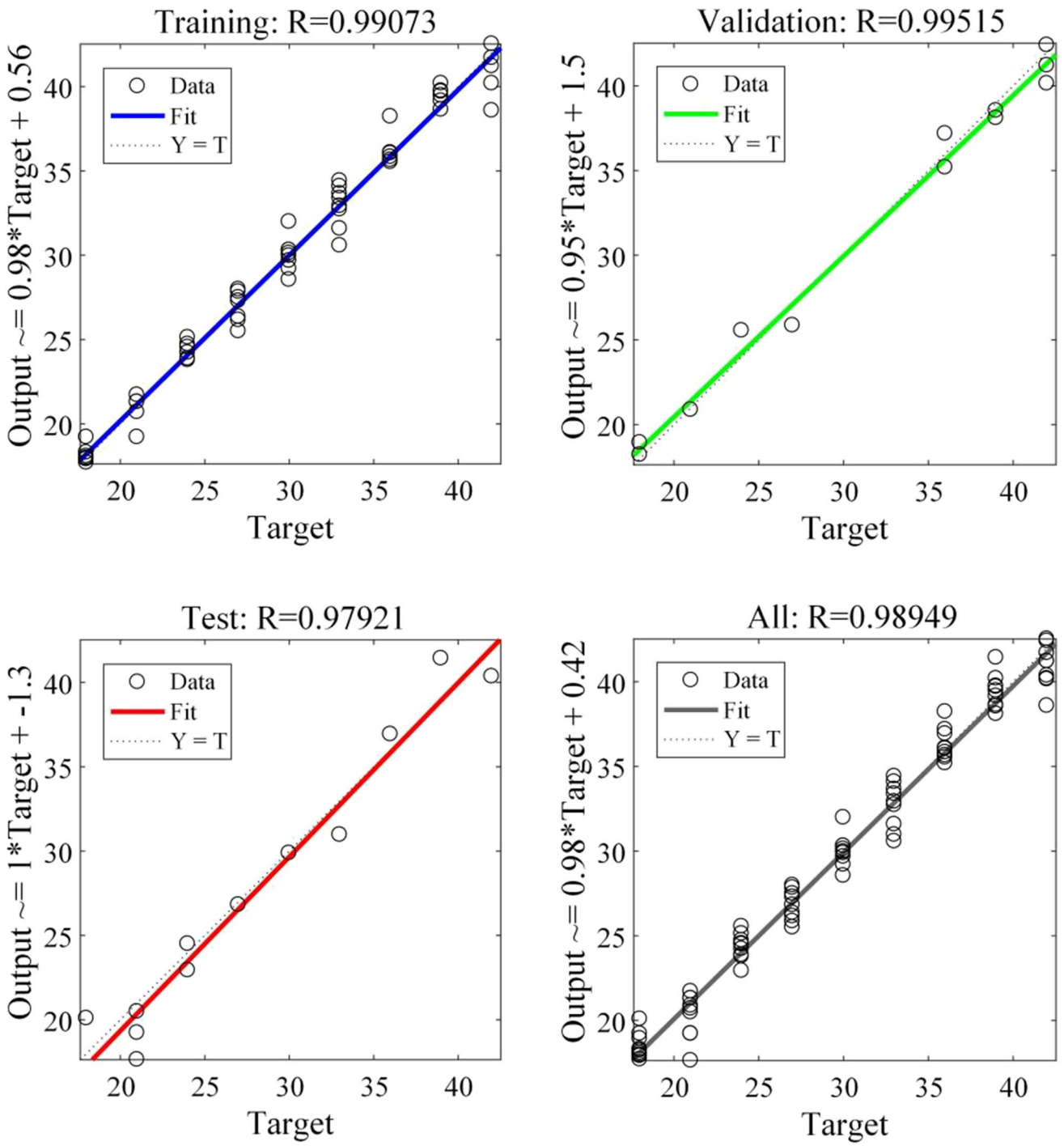


**Fig. 12** Regression analysis of the BP neural network model with output of traverse speed

experiments were randomly assigned within the prediction range of the BP neural network model. As shown in Table 6, the error between predictive milling depth and measured milling depth can be controlled to less than 7% of the total milling depth. With the BP neural network model, the traverse speed required for predictive milling depth can be obtained accurately.

### 3.5 Aspheric processing

Aspheric processing of RB-SiC was performed. The processing area was a ring with an inner diameter of 40 mm and outside diameter of 160 mm. The generatrix of aspherical surface was parabola, and its equation (Eq. 1) was characterized by a depth $D$ and a radial distance $R$.

**Table 6** Validation experiments of the BP neural network model with output of traverse speed

| Run | Predictive milling depth (μm) | Step-over distance (mm) | Predictive traverse speed (mm/s) | Measured milling depth (μm) | Error |
|---|---|---|---|---|---|
| 1 | 280 | 0.44 | 32.40 | 281 | 0.36% |
| 2 | 480 | 0.38 | 24.46 | 449 | 6.46% |
| 3 | 400 | 0.24 | 41.46 | 425 | 6.25% |
| 4 | 750 | 0.30 | 18.84 | 747 | 0.40% |
| 5 | 370 | 0.27 | 40.98 | 372 | 0.54% |
| 6 | 220 | 0.46 | 37.66 | 233 | 5.91% |
| 7 | 750 | 0.21 | 26.25 | 785 | 4.67% |
| 8 | 180 | 0.56 | 36.62 | 184 | 2.22% |

$$D = \left(0.1 \times R^2 - 840\right) \times 10^{-3} \quad (1)$$

The unit of $D$ and $R$ was millimeter. The minimum milling depth was 200 μm at the outer circle, and the maximum milling depth was 800 μm at the inner circle. The processing path (Fig. 13) was composed of 20 spiral segments to obtain twenty milling depths each differing by 30 μm. The step-over distance and traverse speed (Table 7) were obtained on the basis of BP neural network models. The result of aspheric processing is presented in Fig. 14.

## 4 Results and discussion

### 4.1 Surface roughness analysis of pockets

The surface roughness Ra and Rz at the bottom of the pockets is measured to analyze the effect of traverse speed and step-over distance on surface quality. Due to the large surface roughness, no filtering is done to avoid damaging the initial face shape. The surface roughness of five areas of 600 μm × 600 μm at the bottom of the pocket was measured and averaged.

The effect of step-over distance on surface roughness is presented in Fig. 15. The results show that as step-over distance decreases, the surface roughness slightly decreases when the step-over distance is in the range from 0.45 to 0.6 mm and obviously increases when the step-over distance is less than 0.45 mm. The step-over distance of 0.6 mm at traverse speed of 30 mm/s corresponds to the step-over distance of 1.8σ on linear superposition (Fig. 2b) of the Gaussian curves which slight surface waviness presents. The slight surface waviness leads to slight increase on surface roughness. Therefore, the surface roughness is slightly decreased by decreasing the step-over distance in the range between 0.45 and 0.6 mm. As the step-over distance decreases, the secondary impact of abrasives increases. This leads to the increase on surface roughness when the step-over distance is less than 0.45 mm.

The effect of traverse speed on surface roughness is presented in Fig. 16. The results show that as the traverse speed decreases, the surface roughness changed a little when traverse speed is larger than 30 mm/s and obviously increases when traverse speed is less than 30 mm/s. When the traverse speed is larger than 30 mm/s, the milling depth of the single kerf is relatively small, and its variation has less impact on the secondary impact of abrasive, so the surface roughness is changed a little. When traverse speed is less than 30 mm/s, the milling depth of the single kerf increases rapidly as the traverse speed decreases, resulting in the rapid increase of

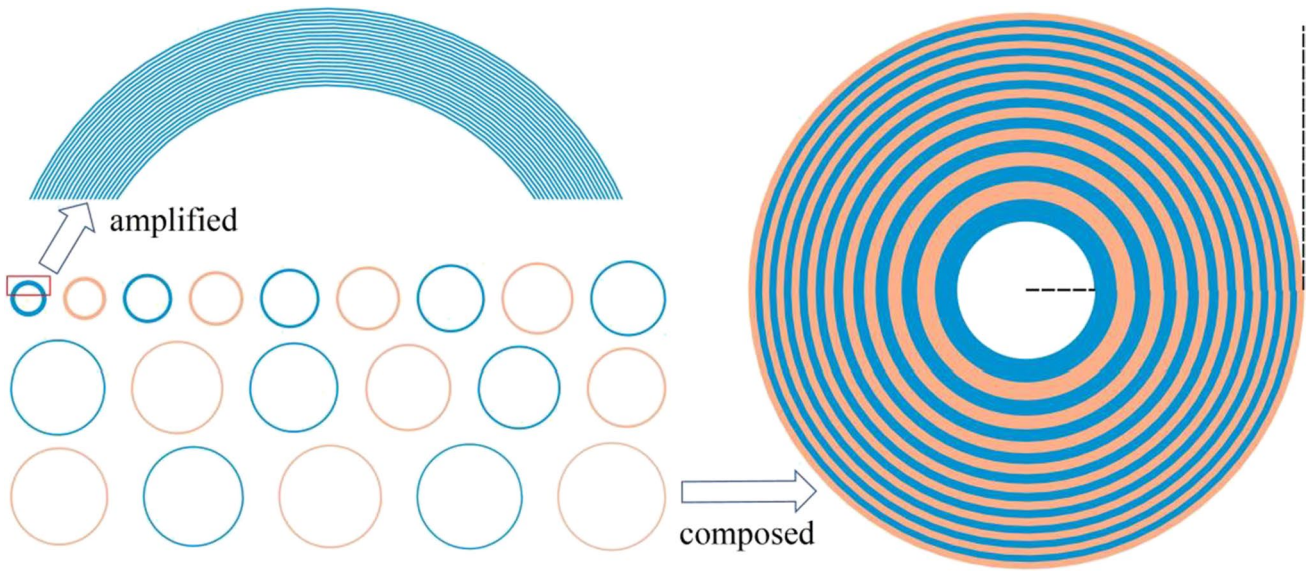


**Fig. 13** Processing path of abrasive water jet milling

**Table 7** Details of aspheric processing

| Run | Milling depth (μm) | Radius of ring (mm) | Width of ring (mm) | Traverse speed (mm/s) | Step-over distance (mm) | Number of Loops | Rounding off | Adjusted step-over distance (mm) | Adjusted traverse speed (mm/s) |
|---|---|---|---|---|---|---|---|---|---|
| 1 | 200 | 78.10–80.00 | 1.898 | 40.000 | 0.474 | 4.001 | 4 | 0.474 | 40.248 |
| 2 | 230 | 76.16–78.10 | 1.945 | 39.000 | 0.434 | 4.478 | 4 | 0.486 | 34.278 |
| 3 | 260 | 74.16–76.16 | 1.996 | 38.000 | 0.397 | 5.032 | 5 | 0.399 | 39.549 |
| 4 | 290 | 72.11–74.16 | 2.051 | 36.000 | 0.376 | 5.458 | 5 | 0.410 | 33.475 |
| 5 | 320 | 70.00–72.11 | 2.111 | 35.000 | 0.355 | 5.948 | 6 | 0.352 | 36.536 |
| 6 | 350 | 67.82–70.00 | 2.177 | 34.000 | 0.338 | 6.444 | 6 | 0.363 | 31.910 |
| 7 | 380 | 65.57–67.82 | 2.249 | 33.000 | 0.326 | 6.899 | 7 | 0.321 | 33.793 |
| 8 | 410 | 63.25–65.57 | 2.329 | 32.000 | 0.322 | 7.241 | 7 | 0.333 | 30.523 |
| 9 | 440 | 60.83–63.25 | 2.418 | 31.000 | 0.322 | 7.511 | 8 | 0.302 | 31.783 |
| 10 | 470 | 58.31–60.83 | 2.518 | 30.000 | 0.322 | 7.811 | 8 | 0.315 | 28.991 |
| 11 | 500 | 55.68–58.31 | 2.632 | 29.000 | 0.320 | 8.237 | 8 | 0.329 | 26.491 |
| 12 | 530 | 52.92–55.68 | 2.763 | 28.000 | 0.313 | 8.835 | 9 | 0.307 | 27.250 |
| 13 | 560 | 50.00–52.92 | 2.915 | 27.000 | 0.303 | 9.621 | 10 | 0.292 | 27.734 |
| 14 | 590 | 46.90–50.00 | 3.096 | 26.000 | 0.292 | 10.591 | 11 | 0.281 | 27.896 |
| 15 | 620 | 43.59–46.90 | 3.315 | 25.000 | 0.283 | 11.731 | 12 | 0.276 | 27.361 |
| 16 | 650 | 40.00–43.59 | 3.589 | 24.000 | 0.276 | 13.013 | 13 | 0.276 | 26.290 |
| 17 | 680 | 36.06–40.00 | 3.944 | 23.000 | 0.275 | 14.349 | 14 | 0.282 | 24.689 |
| 18 | 710 | 31.62–36.06 | 4.433 | 22.000 | 0.282 | 15.736 | 16 | 0.277 | 24.032 |
| 19 | 740 | 26.46–31.62 | 5.165 | 21.000 | 0.294 | 17.599 | 18 | 0.287 | 22.195 |
| 20 | 770 | 20.00–26.46 | 6.458 | 20.000 | 0.304 | 21.263 | 21 | 0.308 | 19.529 |

**Fig. 14** Aspherical RB-SiC surface processed by abrasive water jet milling

the secondary impact of abrasive. This leads to the increase of surface roughness when the traverse speed is less than 30 mm/s.

## 4.2 Measurement and evaluation of aspheric surface

Four profiles (Fig. 17) on processed RB-SiC were extracted at per 45° and compared with the generatrix of the aspherical surface. The extracted profiles are highly

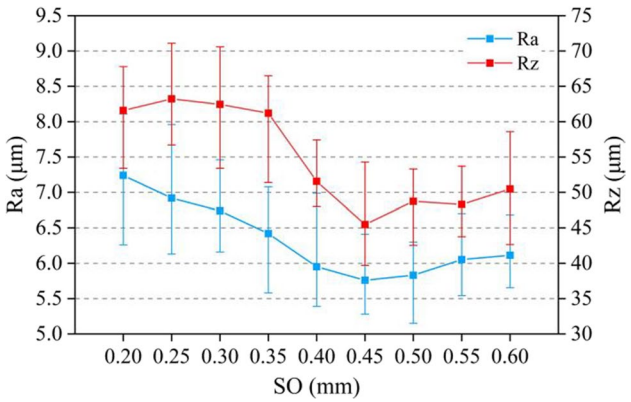


**Fig. 15** Effect of step-over distance on surface roughness with a traverse speed of 30 mm/s

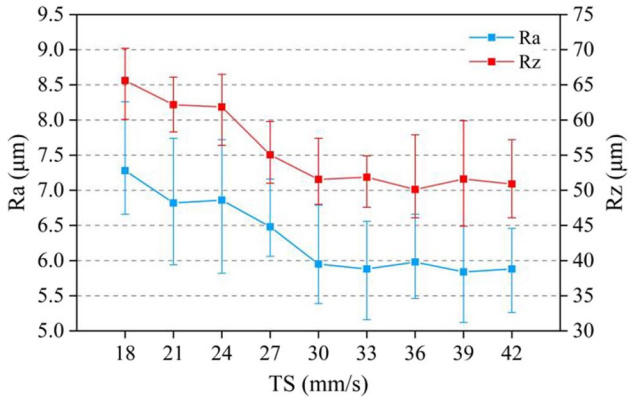


**Fig. 16** Effect of traverse speed on surface roughness with a step-over distance of 0.4 mm

fitted to the generatrix of aspherical surface. Most of processing allowance can be removed by this method; thus, the grinding allowance for subsequent grinding can be effectively reduced.

The error curves (Fig. 18) which are the difference between extracted profiles and the generatrix of aspherical surface are controlled at about 160 μm, 20% of the total depth. The maximum error is about 10% of the total depth. The error curves float at the zero line. This indicates that the overall deviation of milling depth predicted by BP neural network models is small. The error is small when the milling depth is small, and the error increases gradually when the milling depth gradually increases. Error at large milling depth is more prone to increase the maximum error and increase the subsequent grinding depth.

The maximum error is about 10% of the total depth, larger than the predictive error of the BP neural network models. The reasons are as follows: The average depth was used to represent the error in BP neural network models, and the actual surface profile was adopted to represent the error of aspheric processing. This leads to the larger error in aspheric processing than BP neural network models.

Considering the error of aspheric processing and the removal of cracks produced by abrasive water jet, the subsequent design grinding depth should be greater than 150 μm. The proportion of processing allowance removed by abrasive water jet is related to the total depth of the processing allowance. As the total processing allowance increases, the proportion of the processing allowance removed by the abrasive water jet increases. The material

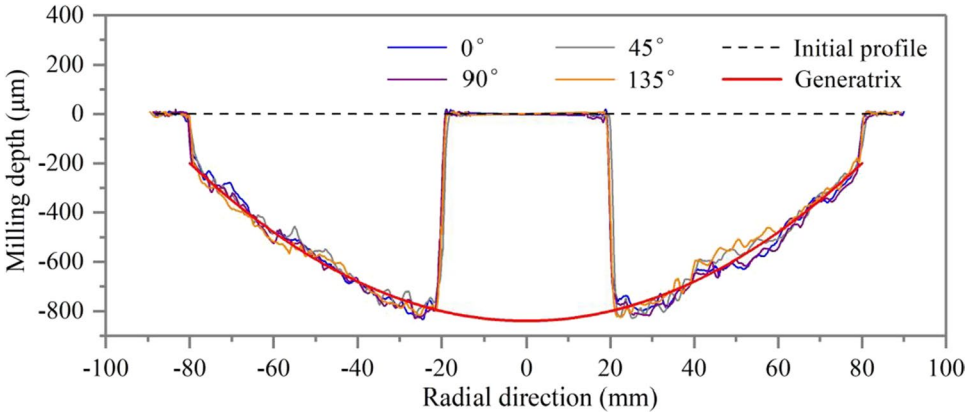


**Fig. 17** Comparison of surface profiles with the generatrix

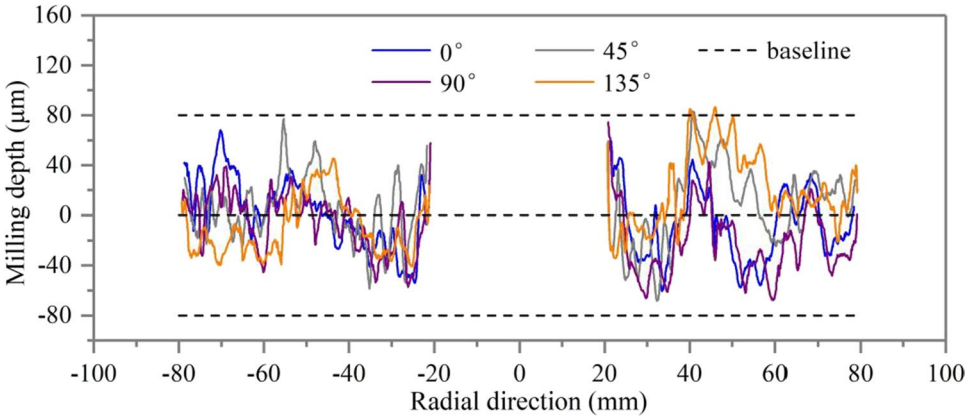


**Fig. 18** The error curves of aspheric processing

removal rate is calculated as 4.91 $mm^3/s$, approximately 10 times higher than grinding efficiency [25, 26]. Due to the limitation of low constant pressure and small nozzle diameter in this experiment, the material removal rate is largely limited. The material removal rate still has a high room for improvement.

By using BP neural networks to control milling depths and setting different milling depths in spiral processing path, the aspheric surface can be accurately processed by abrasive water jet. This method can be applied to the processing of mirrors for rapid material removal to reduce total processing cycle. This method could also be applied in fields where milling depth processed by abrasive water jet needs to be accurately controlled.

## 5 Conclusion

In this study, a method to quickly reduce the processing allowance in large diameter RB-SiC mirror blanks using abrasive water jet milling was presented. The single kerf profile processed by abrasive water jet milling was effectively fitted to the Gaussian curve. Linear superposition of multiple Gaussian curves with overlapping step-over distance was performed. The surface waviness of the linear superimposed curve was reduced by reducing step-over distance. By establishing BP neural network models, the milling depth can be accurately predicted. Aspheric processing of RB-SiC by abrasive water jet milling was performed. The processed surface was highly fitted to the design aspheric surface. By using abrasive water jet milling, the processing allowance of large diameter RB-SiC mirror blank can be effectively reduced. The following conclusions can be drawn from the study:

(1) The single kerf profile processed by abrasive water jet milling was effectively fitted to the Gaussian curve, and σ of the Gaussian curve was obtained to represent step-over distance. Linear superposition of multiple Gaussian curves with overlapping step-over distance was performed. The surface waviness of linear superimposed curve was reduced by reducing step-over distance and almost removed when $SO = 1.5\sigma$. When the linear superposition of Gaussian curves is combined with the machining accuracy of abrasive water jet milling, the surface waviness on the processed surface can be effectively reduced when the step-over distance is controlled to less than $1.8\sigma$.

(2) Due to high influence of step-over distance and traverse speed on milling depth and ease of control, step-over distance and traverse speed were chosen to control milling depth. The BP neural network models with step-over distance and traverse speed as parameters were established to predict milling depth. The BP neural network models are reliable, and the prediction error can be controlled to about 5% of the total depth, with a maximum error less than 7% of the total depth.

(3) Aspheric processing of RB-SiC with a processing path composed of 20 spiral segments was performed by abrasive water jet milling. The processing area was a ring with 40 mm inner diameter and 160 mm outside diameter. Different milling depths were obtained by controlling step-over distance and traverse speed. The processed aspherical surface was highly fitted to the design aspherical surface with a maximum error of about 10% of the total depth. The error curves float at the zero line, and the error curves were controlled at 20% of the total depth. The material removal rate is calculated approximately 10 times higher than grinding efficiency. The material removal rate still has a high room for improvement. By this method, the processing allowance of large diameter RB-SiC mirror blanks can be effectively reduced. This method could also be applied in fields where milling depth processed by abrasive water jet needs to be accurately controlled.

**Author contribution** Hongxing Deng: conceptualization, methodology, validation, formal analysis, investigation, writing—original draft. Peng Yao: resources, writing—review and editing, funding acquisition, data curation. Kuo Hai: resources, writing—review and editing. Shimeng Yu: resources and review. Chuanzhen Huang: resources, project administration. Hongtao Zhu: formal analysis, writing—review and editing. Dun Liu: resources, data curation.

**Funding** This work was supported by the National Natural Science Foundation of China (No. 52075302), the National Key R&D Program of China (No. 2021YFB3203100), and the Shenzhen Science and Technology Program (No. GJHZ20210705142537003).

**Data availability** Transparent.

**Code availability** Not applicable.

## Declarations

**Ethical approval** The author obliged all the rules regarding the ethic in publication.

**Consent to participate** All the authors consent regarding the data provided in the text as well as the order of authorship.

**Consent for publication** All the authors consent regarding publication immediately after acceptance.

**Competing interests** The authors declare no competing interests.

## References

1. Wang ZS, He X, Fu LL (2014) Design of large size circular primary mirror of space camera. Infrared 35(09):15–18
2. Li ZD, Liu HY, Wei JH, Li YJ, Sun SL (2020) Research on stress of large aperture mirror supporting structures by search algorithm. Acta Opt Sin 40(14):135–143

3. Tao XP (2015) Precise alignment method of online optical testing for large-aperture mirror fabrication. Chin Opt 8(06):1027–1034
4. San B, Li JL, Sun B (2015) Light-weight technology and its application of large-aperture mirror in space camera. Infrared Laser Eng 44(10):3043–3048
5. Wang XK (2015) Optical design of a high resolution space camera. Acta Opt Sin 35(01):329–337
6. Yan Y, Jin G (2011) Material preparation, surface modification and aspheric processing of RB-SiC mirrors. Opt Precis Eng 19(08):1750–1756
7. Zhang ZY, Yang X, Zheng LG, Xue DL (2017) High-performance grinding of a 2-m scale silicon carbide mirror blank for the space-based telescope. Int J Adv Manuf Technol 89(1–4):463–473
8. Saurabh S, Tiwari T, Nag A, Dixit AR, Mandal N, Das AK, Mandal A, Srivastava AK (2018) Processing of alumina ceramics by abrasive water jet- an experimental study. Mater Today Proc 5(9):18061–18069
9. Schwartzentruber J, Spelt JK, Papini M (2018) Modelling of delamination due to hydraulic shock when piercing anisotropic carbon-fiber laminates using an abrasive water jet. Int J Mach Tools Manuf 132:81–95
10. Akıncıoğlu S (2021) Investigation of effect of abrasive water jet (AWJ) machining parameters on aramid fiber-reinforced polymer (AFRP) composite materials. Aircr Eng Aerosp Technol 93(4):615–628
11. AltinKarataş M, Gökkaya H, Akincioğlu S, Biberci M (2022) Investigation of the effect of AWJ drilling parameters for delamination factor and surface roughness on GFRP composite material. Multidiscip Model Mater Struct 18(4):734–753
12. Tabatchikova TI, Tereshchenko NA, Yakovleva IL, Gudnev NZ (2018) Structure of near-surface layer of high-strength steel subjected to abrasive waterjet cutting. Phys Met Metallogr 119(9):871–879
13. Sultan T, Gilles P, Cohen G, Cenac F, Rubio W (2016) Modeling incision profile in AWJM of titanium alloys Ti6Al4V. Mech Ind 17(4):403
14. Carrascal A, Alberdi A (2010) Evolutionary industrial physical model generation. International Conference on Hybrid Artificial Intelligence Systems 6076:327–334
15. Meng HC, Ludema KC (1995) Wear models and predictive equations: their form and content. Wear 181–183(32):443–457
16. Zeng JY, Kim TJ (1996) An erosion model of polycrystalline ceramics in abrasive waterjet cutting. Wear 193(2):207–217
17. Pahuja R, Ramulu M (2019) Abrasive water jet machining of titanium (Ti6Al4V)-CFRP stacks - a semi-analytical modeling approach in the prediction of kerf geometry. J Manuf Process 39:327–337
18. Mohankumar V, Kanthababu M (2020) Semi-empirical model for depth of cut in abrasive waterjet machining of metal matrix composites. J Braz Soc Mech Sci Eng 42:507
19. Ozcan Y, Tunc LT, Kopacka J, Cetin B, Sulitka M (2021) Modelling and simulation of controlled depth abrasive water jet machining (AWJM) for roughing passes of free-form surfaces. Int J Adv Manuf Technol 114:3581–3596
20. Wang YF, Yang ZG (2008) Finite element model of erosive wear on ductile and brittle materials. Wear 265(5–6):871–878
21. Anwar S, Axinte DA, Becker AA (2013) Finite element modelling of abrasive waterjet milled footprints. J Mater Process Technol 213(2):180–193
22. Anwar S, Axinte DA, Becker AA (2013) Finite element modelling of overlapping abrasive waterjet milled footprints. Wear 303(1–2):426–436
23. Bui VH, Gilles P, Sultan T, Cohen G, Rubio W (2017) A new cutting depth model with rapid calibration in abrasive water jet machining of titanium alloy. Int J Adv Manuf Technol 93:1499–1512
24. Wang ZS, Zhang JX, Wang JX, He X, Fu LL, Tian FX, Liu XF, Zhao YC (2019) A back propagation neural network based optimizing model of space-based large mirror structure. Optik 179:780–786
25. Huang SQ, Wei ZZ, Rao XS, Li C, Zhang FH (2021) Optimization of processing parameters during electrical discharge diamond grinding of RB-SiC ceramics based on grey relational theory. Diamond Abras Eng 41(06):56–62
26. Yin LH, Wang XK, Li LX, Li LF, Zhang ZY, Zheng LG, Zhang XJ (2015) Fast grinding of large SiC off-axis aspheric surface. Opt Precis Eng 23(09):2497–2505